

The role of the second virial coefficient in the vapor-liquid phase coexistence of anisotropic square-well particles

Péter Gurin^a, Szabolcs Varga^{a*} and Gerardo Odriozola^b

^a*Physics Department, Centre for Natural Sciences, University of Pannonia, PO Box 158, Veszprém, H-8201 Hungary*

^b*Area de Física de Procesos Irreversibles, División de Ciencias Básicas e Ingeniería,*

Universidad Autónoma Metropolitana-Azcapotzalco, Av. San Pablo 180,

02200 México, D. F., Mexico.

We examine the role of the second virial coefficient in the vapor-liquid (VL) phase coexistence of anisotropic hard bodies with square-well attractions of variable range. According to the extended law of corresponding states, the parameters of hard body interactions and attractions can be built into the reduced density and the reduced second virial coefficients, respectively, which gives rise to the collapse of all VL binodals in the reduced second virial coefficient vs. reduced density plane. The second virial perturbation theory shows that the shape dependence appears as an extra parameter in the phase behavior of anisotropic particles, which does not make possible the perfect collapse of the VL binodals for varying shapes. Interestingly, the binodal curves go closely together and even cross each other in the liquid side allowing to define a quasi-master curve. The existence of an almost perfect master curve is confirmed by replica-exchange Monte Carlo simulations for oblate square-well ellipsoids with several shape anisotropies.

*Corresponding author.

E-mail address: vargasz@almos.uni-pannon.hu (S. Varga).

I. Introduction

In the progress of understanding the liquid state of matter, it was a milestone when it turned out that the structure of simple liquids is determined primarily by hard-core repulsive interactions, while the emergence of vapor-liquid (VL) phase coexistence is due to the attractions between the particles [1]. These findings constitute the basis of perturbation theories of simple fluids, where the hard body part of the interactions forms the reference system, and the effects of attraction are taken into account as a perturbation [1, 2]. The outstanding role of Douglas Henderson (alias Doug) together with John Adair Barker was unquestionable in the development of the second-order perturbation theory for simple fluids, which can describe the phase behavior

of hard bodies with both short and long-range attractions [3, 4]. The Barker-Henderson perturbation theory is nowadays a standard statistical mechanical tool for simple fluids [5, 6] and it is built into other theories such as the statistical association fluid theory [7] and the classical density functional theory of inhomogeneous fluids [8]. In addition, Doug contributed in many fields of statistical mechanics to understand the nature of both liquids and electrolyte solutions in bulk and confinement [9-17]. In connection with this work, he developed a new equation of state for hard bodies [18], which served as a basis for a better description of anisotropic convex particles [19], and he also contributed to the extension of van der Waals (VDW) theory for mixtures [20]. In memory of Doug, we examine the VDW corresponding states of anisotropic particles with both perturbation theory and simulation.

On the level of VDW theory, the thermodynamic quantities (density, temperature, and pressure) can be reduced in such a way that all substances satisfy the same equation of state. Moreover, two fluids are in the same corresponding state if they possess the same reduced macroscopic variables, where the reduction is carried out with the critical properties of the VL transition. Many substances follow the law of corresponding states, but there are exceptions [21]. Strictly speaking, only the conformal pair potentials obey this law, while the non-conformal ones like the square-well pair potential do not [22]. Therefore, it was a surprising observation that the critical value of the reduced second virial coefficient for short-range pair potentials does not depend on the details of the attraction, i.e. it is the same for conformal and non-conformal ones [23]. This observation initiated Noro and Frenkel to devise an extended law of corresponding states (ELCS) [24]. According to this law the thermodynamic properties of all short-range spherically symmetric pair potentials are identical when compared at the same reduced density and second virial coefficient. The ELCS implies that the effect of the particle's diameter and the attraction range can be incorporated into the reduced density and the reduced second virial coefficient, respectively. In the case of square-well interaction, the law works well for short-range attraction. In the sticky limit of this potential, the ELCS can be proved exactly [25-27]. However, the validity of the ELCS is questionable even for non-sticky short-range attractive interactions because the second virial coefficient corresponding to the VL critical point depends linearly on the attraction range [28, 29]. Curiously, these findings have negligible effects on the critical temperature due to the highly nonlinear relationship between the variables. Therefore, it is reasonable to assume that the reduced second virial coefficient is constant at the critical point for very short-range attractions [30-33].

The ELCS was extended for anisotropic pair potentials, where the interaction is directional and short-range [34]. In addition, the relevance of ELCS is pointed out even in the dynamical [35] and morphological properties [36] of different systems showing that these properties depend mainly on the reduced second virial coefficient. A possible reason for the success of the ELCS is that each interacting pair of particles have the same contribution in the partition function in the case of short-range attractions [37]. Regarding the very long-range attractions, where all particles

feel the same mean-field, the second virial contribution becomes identical to the mean-field energy contribution [2]. In this limit, the details of the potential become again irrelevant and the reduced second virial coefficient turns proportional to the inverse of the reduced temperature. Consequently, the reduced second virial coefficient links the short-range and long-range cases. No doubt that the reduced second virial coefficient does incorporate the effects of all particle properties for intermediate-range attractions, but it is worth testing the deviation from both the original law of corresponding states [1] and the ELCS [6, 38, 39].

In this work, we examine the nature of the VL phase transition of anisotropic hard particles embedded into attractive square wells. This way, we look for a link between the very short and long-range limits of the attraction. Along this line, we analyse the VL phase coexistence results of the second virial perturbation theory for several shapes and aspect ratios and search for reduced quantities, which are not sensitive to the values of the particle parameters. In particular, we search for the best representation of the VL binodals that makes the phase coexistence curves collapse into a single master one. The practical benefit of having such a master curve is that the VL phase diagram can be easily constructed from it for several systems. We show that the attractive part of the second virial coefficient along the VL binodal is not sensitive to the actual shape and range of the attractive well. Therefore, all phase diagrams better collapse with this virial coefficient than with the reduced temperature and density in the VDW representation. We test this finding with replica-exchange Monte Carlo simulations, where the VL binodals of 84 different oblate ellipsoid systems are determined by setting the attraction range in between the very short and very long-range mean-field limits. With this choice for the attraction range, we deal with those systems where the role of the second virial coefficient is not trivial.

II. Models

We examine the VL phase coexistence in such anisotropic fluids where particles are modelled as non-spherical hard bodies embedded into attractive square-wells with variable shape and range. In Fig. 1 we show the schematic of some hard bodies (cylinder, spherocylinder, and uniaxial ellipsoids), which are surrounded by attractive square-wells. The shape of the attraction is taken to be identical with the shape of the body. The inner hard cores are not allowed to overlap, while the outer shells attract each other with an anisotropic square-well pair interaction. Therefore the pair interaction energy between two particles with orientations $\vec{\omega}_1$ and $\vec{\omega}_2$, center-to-center distance r_{12} , and center-to-center orientation $\vec{\omega}_{12}$ can be written as

$$u(r_{12}, \vec{\omega}_{12}, \vec{\omega}_1, \vec{\omega}_2) = \begin{cases} \infty, & r_{12} \leq \sigma(\vec{\omega}_{12}, \vec{\omega}_1, \vec{\omega}_2) \\ -\varepsilon, & \sigma(\vec{\omega}_{12}, \vec{\omega}_1, \vec{\omega}_2) < r_{12} \leq \sigma_o(\vec{\omega}_{12}, \vec{\omega}_1, \vec{\omega}_2), \\ 0, & r_{12} > \sigma_o(\vec{\omega}_{12}, \vec{\omega}_1, \vec{\omega}_2) \end{cases} \quad (1)$$

where ε is the well-depth. Moreover, $\sigma(\vec{\omega}_{12}, \vec{\omega}_1, \vec{\omega}_2)$ and $\sigma_o(\vec{\omega}_{12}, \vec{\omega}_1, \vec{\omega}_2)$ are contact distances of the inner hard-core and the outer attractive square-well shells, respectively. These contact distances also depend on the lengths and the shape of the particle (see Fig. 1). As the outer attraction shell encloses the inner repulsive one, we prescribe that $\sigma_o \geq \sigma$. We change the shape and the side lengths of the particle through σ , while σ_o is varied to tune the range and the shape of the attraction.

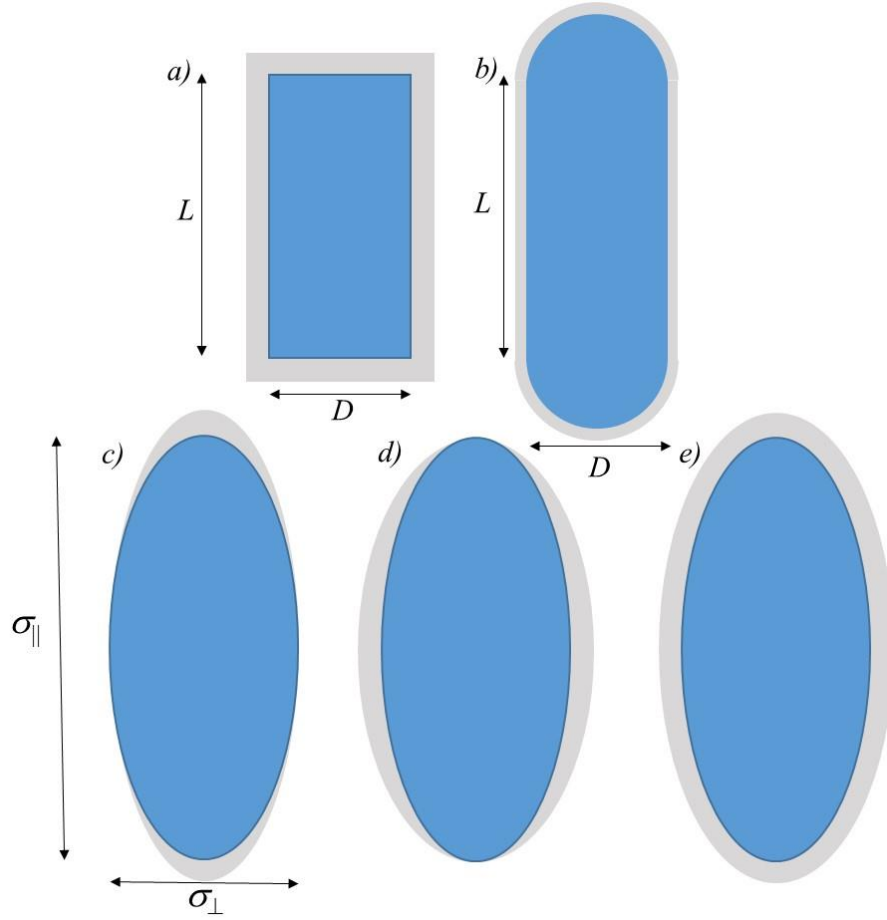


Figure 1. Hard nonspherical particles embedded into attractive square-wells: a) cylinder with length L and diameter D , b) spherocylinder with length $L+D$ and diameter D and c)-d) ellipsoids with σ_{\parallel} major and σ_{\perp} minor lengths. The type of attractions: c) pole, d) equator, and e) uniform. The hard objects are filled with blue colour, while the grey shaded regions represent the outer attraction shell.

III. Theory

The free energy of non-spherical particles with surrounding square-well attractions can be written as a sum of ideal, hard body, and attractive contributions. Although we have a quite accurate knowledge about the hard body and square-well terms for spherical particles [3, 40-46], only few theoretical and simulation studies are devoted to treat these terms for nonspherical ones

[47-50]. The hard body contribution can be approximated accurately with the Parsons-Lee rescaling formula [47, 48], while the second-virial perturbation term of the virial expansion can account for the attractive contribution [49]. It is an important feature of this perturbation theory that it incorporates exactly the second virial coefficient of the pair potential. On the level of the applied approximations, the free energy density is given by

$$\frac{\beta F}{N} = \ln \eta - 1 + \frac{4\eta - 3\eta^2}{4(1-\eta)^2} \frac{B_2^H}{v} + \eta \frac{B_2^A}{v}, \quad (2)$$

where $\beta = \frac{1}{k_B T}$ is the inverse temperature, $\eta = \rho v$ is the packing fraction, $\rho = N/V$ is the number density, v is the volume of the hard body, B_2^H is the second virial coefficient of the hard body interactions, and B_2^A is the attractive part of the complete second virial coefficient. Eq. (2) shows that the details of the interaction (particle's shape, ranges of inner and outer shells) are incorporated into B_2^H/v and B_2^A/v terms. From this dependence we can conclude that two systems are in the same reduced state on the level of the applied perturbation theory when both have the same η , B_2^H/v , and B_2^A/v values. A consequence of having the same reduced quantities is that the phase behaviours of the corresponding systems are identical in the reduced parameter space. It is easy to show for hard bodies with attractions that $B_2 = B_2^H + B_2^A$, where B_2 is the second virial coefficient. Note that B_2^A can be written down analytically for the square-well attraction in the following form

$$B_2^A = \left(1 - e^{\beta \varepsilon}\right) \left(B_2^O - B_2^H\right). \quad (3)$$

In this equation, the outer contact distance (σ_o) determines B_2^O , while the inner hard body one (σ) gives B_2^H . Later in this section we will provide explicit expressions for B_2^H and B_2^O for the shapes shown in Fig. 1.

The pressure (P) and the chemical potential (μ) can be obtained from the free energy density using the standard thermodynamic relationships. They can be written in dimensionless form as follows

$$\beta P v = \eta^2 \frac{\partial \beta F / N}{\partial \eta}, \quad (4)$$

$$\beta \mu = \frac{\beta F}{N} + \frac{\beta P v}{\eta}. \quad (5)$$

To understand the nature of the VL phase coexistence, it is useful to determine the spinodal curve from the $\frac{\partial \beta P v}{\partial \eta} = 0$ condition. After substitution of Eq. (2) into Eq. (4) and using the spinodal condition, we get that

$$b_2^A = \frac{\eta - 4}{4(1-\eta)^4} b_2^H - \frac{1}{2\eta}, \quad (6)$$

where $b_2^A = B_2^A / v$ and $b_2^H = B_2^H / v$ are the reduced attractive and hard body terms of B_2 , respectively. Eq. (6) shows that b_2^A is negative along the spinodal and it is a unique function of the packing fraction for a given hard-core interaction b_2^H . This means that b_2^A vs. η curves do not depend on the details of the attractive interactions, i.e. the spinodals of different attractive shells fall into the same master curve. The critical values of η and b_2^A are the other important properties of VL phase coexistences, which can be obtained from the following thermodynamic conditions

$$\begin{aligned} \frac{\partial \beta P v}{\partial \eta} &= 0, \\ \frac{\partial^2 \beta P v}{\partial \eta^2} &= 0. \end{aligned} \quad (7)$$

Using Eqs. (2), (4), and (7) we can determine η_c and $b_{2,c}^A$, which are the critical values of η and b_2^A . After straightforward calculations, we get that

$$b_{2,c}^A = \frac{\eta_c - 4}{(1-\eta_c)^4} \frac{b_2^H}{4} - \frac{1}{2\eta_c}, \quad (8)$$

where η_c satisfies

$$\frac{2(1-\eta_c)^5}{3\eta_c^2(5-\eta_c)} = b_2^H. \quad (9)$$

Eqs. (8) and (9) indicate that η_c and $b_{2,c}^A$ depend on b_2^H , i.e. only the hard body shape and the aspect ratio have effects on the critical properties. Note that the parameters of the attractive interaction do not appear in Eqs. (8) and (9). We solve Eq. (9) numerically for cylinders,

spherocylinders, and ellipsoids. Using Eqs. (3), (8), and (9) we can obtain the critical temperature for various square-well attractions as follows

$$\frac{1}{T_c^*} = \ln \left\{ 1 - \frac{b_{2,c}^A}{b_2^O - b_2^H} \right\}, \quad (10)$$

where $T_c^* = k_B T_c / \varepsilon$ is the dimensionless critical temperature and $b_2^O = B_2^O / v$. Note that $b_{2,c}^A$ is the result of Eqs. (8) and (9). In addition to the spinodal and the critical properties, we determine the VL binodal using the phase equilibrium conditions, which states that the pressures and chemical potentials of the vapor (V) and the liquid (L) phases must satisfy $P_V = P_L$ and $\mu_V = \mu_L$. Solving these equations we find the coexisting V and L packing fractions at a given b_2^H and b_2^A . Therefore, the VL binodal also forms a master curve in the b_2^A vs. η plane for a given hard-core shell (b_2^H). We present the binodals and spinodals together in the Results section. We restrict our attention to those cases where the shape of the inner and the outer shells are identical, but the aspect ratios can be different (see Fig. 1). Our theoretical and simulation studies concern mainly the uniaxial ellipsoidal shape, where the outer square-well shell surrounds the inner repulsive one. Moreover, we consider other uniaxial shapes like cylinders and spherocylinders. For any uniaxial shapes, the reduced second virial coefficient of a hard body is only a function of the aspect ratio (k), i.e. $b_2^H = b_2(k)$, where k is the ratio of parallel and the perpendicular lengths to the rotational symmetry axis of the uniaxial body. In the case of the ellipsoidal shape it can be shown [51] that

$$b_2(k) = 1 + \frac{3}{4} \left[1 + \frac{\tanh^{-1} \left(\frac{\sqrt{k^2 - 1}}{k} \right)}{k \sqrt{k^2 - 1}} \right] \left\{ 1 + \frac{k^2}{\sqrt{k^2 - 1}} \tan^{-1} \left(\sqrt{k^2 - 1} \right) \right\}, \quad (11)$$

where the aspect ratio is given by $k = \frac{\sigma_{\parallel}}{\sigma_{\perp}}$ and σ_{\parallel} (σ_{\perp}) is the length parallel (perpendicular) to the main symmetry axis of the ellipsoid. Note that $k > 1$ for prolate shapes and $0 < k < 1$ for oblate ones. The volume of the ellipsoid is given by $v = \frac{\pi}{6} \sigma_{\perp}^2 \sigma_{\parallel}$. The reduced second virial coefficient is also an analytical function of k for cylinders [52] as

$$b_2(k) = \frac{3+\pi}{2} + \frac{\pi}{4k} + k. \quad (12)$$

Using the length (L) and the diameter (D) of the cylinder, we can write that $k = \frac{L}{D}$ and $0 < k < \infty$.

The volume of the cylinder is given by $v = \frac{\pi}{4} D^2 L$. We get the spherocylinder by adding spherical caps to both ends of the cylinder. Therefore this particle is longer a distance D than the cylinder (see Fig. 1). This modification changes the reduced second virial coefficient, because $b_2(k)$ is now given by [53]

$$b_2(k) = 4 + 3 \frac{(k-1)^2}{2+3(k-1)}, \quad (13)$$

where $k = 1 + \frac{L}{D}$. The volume of the particle is now given by $v = \frac{\pi}{6} D^3 + \frac{\pi}{4} D^2 L$ due to the contribution of the spherical caps. Note that the spherocylinder cannot be oblate, because $L > 0$ and $1 < k < \infty$. In order to determine the critical temperature from Eq. (10), it is necessary to determine the second virial coefficient of the outer shell ($b_2^O = B_2^O / v$), too. To do this, we need the aspect ratio and the volume of the outer shell denoted by k_o and v_o , respectively. Using the reduced second virial coefficient (b_2) for the outer shell, we get $b_2^O = b(k_o) v_o / v$.

IV. Simulation

In addition to theoretical calculations we have performed simulation studies for the vapour-liquid phase coexistence of oblate ellipsoids with different attractive shells such as the pole, equator and uniform (see Fig. 1). The liquid-vapor coexistence densities of attractive square ellipsoids were accessed with the replica exchange Monte Carlo method (REMC) [54-56] as a function of temperature. We consider ten replicas having different temperatures, which sample the region close but below the critical one. The technique includes swap trial moves between replicas at adjacent temperatures. The idea is to allow high-temperature replicas to travel long distances in configuration space, which improves the sampling of an expanded

ensemble defined as $Q_{ext} = \prod_{i=1}^{10} Q_{NVT_i}$. Here, Q_{NVT_i} is the canonical partition function of a

system having N particles, volume V , and temperature T_i . In our implementation, the number of replicas equals the number of sampled ensembles. The acceptance swap probability is set as $P_{acc} = \min(1, \exp[(\beta_j - \beta_i)(U_i - U_j)])$, where $U_i - U_j$ being the potential energy difference and $\beta_i - \beta_j$ is the difference between the reciprocal temperatures between replicas i and j . We employ

prismatic cells having a central liquid slab surrounded by vapor [57]. The largest side is three times larger than the others and is perpendicular to the vapor-liquid interfaces. We consider $N = 1000$ particles, which are randomly and orientationally placed at the center of the cells at the beginning of the simulation. The total packing fraction is around 0.12. We kept the center of mass of the system at the prism center and apply periodic boundary conditions in the three directions. We implement Verlet lists to improve performance [58] and varied maximum displacements and rotations during thermalization to yield acceptance rates close to 0.3. Once we observe a steady state we stop thermalization and start production runs. The liquid and vapor densities are then computed from the profiles avoiding the interfaces. More details on the simulation method are given in our previous work [39].

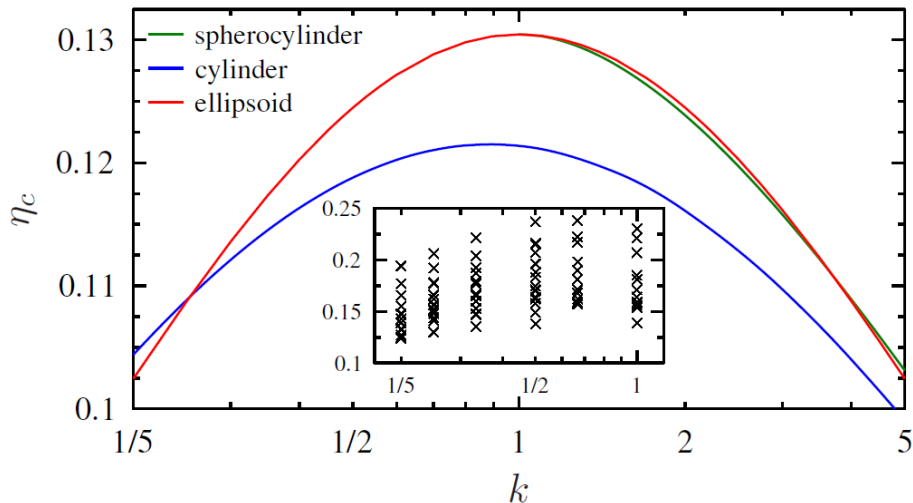


Figure 2. Critical packing fraction of the vapour-liquid phase coexistence as a function of aspect ratio for anisotropic square-well fluids. Curves are the results of Eq. (9) for cylinder, spherocylinder, and ellipsoid shapes. A logarithmic scale is used for k . The inset summaries all of our REMC simulation results for oblate ellipsoids with pole, equator, and uniform attractions.

V. Results

We start this section by analysing the shape dependence of the critical packing fraction of the VL phase transition. In Fig. 2 we show η_c as a function of k for cylinder, spherocylinder, and ellipsoid shapes obtained from Eq. (9) with the corresponding second virial coefficient (see Eqs. (11)-(13)) as $b_2^H = b_2(k)$. It can be seen that the critical packing fraction ranges from 0.1 to 0.13 for $1/5 < k < 5$ and decreases with increasing shape anisotropy. Regarding prolate shapes ($k > 1$), the curves are almost identical for ellipsoids and spherocylinders, while the k dependence of η_c is weaker for cylinders. On the oblate side ($k < 1$), we can observe the lowering of η_c with

decreasing k . Note that $\eta_c(k) = \eta_c(1/k)$ for ellipsoids due to the oblate-prolate symmetry of b_2^H . The same trends can be seen for cylinders without the oblate-prolate symmetry. Our REMC simulation data supports our findings for the k dependence of η_c (see the inset of Fig. 2), which is obtained for oblate ellipsoids. However, the simulation results reveal some weaknesses of the perturbation theory, because η_c depends on the range and the shape of the attraction. We point out later that these discrepancies of the theory are not crucial in the construction of master curve. It is also noteworthy that the simulations do not show nematic ordering in the liquid phase, i.e. the possible isotropic-nematic phase transition does not influence the stability of the VL phase coexistence of the examined systems.

According to the ELCS, the B_2 of the spherical symmetric pair potentials reduced with the corresponding hard sphere second virial coefficient (B_2^{HS}) is practically independent of the potential function for very short-ranged attractions at the VL critical point. Indeed, it is observed that $B_{2,c}/B_2^{HS}$ is about -1.5 at the critical temperature for several spherically symmetric particles with short-ranged attractions [23, 24], where $B_{2,c}$ is the critical second virial coefficient. Note that this condition corresponds to $B_{2,c}^A/B_2^{HS} = -2.5$ as $B_2 = B_2^{HS} + B_2^A$. Now, we focus on the $B_{2,c}^A/B_2^H$, which becomes $B_{2,c}^A/B_2^{HS}$ in the spherical limit ($k=1$). After substituting Eq. (9) into Eq. (8), it is easy to show that

$$\frac{B_{2,c}^A}{B_2^H} = \frac{\eta_c^2 - 5\eta_c - 2}{2(1-\eta_c)^5}. \quad (14)$$

Note that $B_{2,c}^A/B_2^H$ is identical to $b_{2,c}^A/b_2^H$. Eq. (14) shows that the ELCS is valid for a given aspect ratio as the critical packing fraction depends only on k (see Eq. (9)). Consequently, $B_{2,c}^A/B_2^H$ is a constant for a given k and the details of the attractive interaction (the range, the shape, and its depth) affect the VL binodal only through b_2^A . In other words, we can say that $B_{2,c}^A/B_2^H$ is invariant at the critical point, but T_c changes with the shape and range of the attraction. Note that the ELCS is valid for both short and long-ranged attractions on the level of our second virial perturbation theory. In the examined range of the aspect ratio ($1/5 < k < 5$), we find $-2.15 < B_{2,c}^A/B_2^H < -2.65$. In the spherical limit ($k=1$), we get $B_{2,c}^A/B_2^H \approx -2.65$, which is slightly lower than $B_{2,c}^A/B_2^H \approx -2.5$ coming from simulation studies for fluids with short-ranged attractions. As shown in [28], the critical temperature is not very sensitive to the used value of

$b_{2,c}^A$ in Eq. (10). We show the predictive power of the second virial perturbation theory for attractive oblate ellipsoids by comparing the critical temperatures of the theory and REMC simulations. From the several possible attractive wells, we consider pole, equator, and uniform square-well attractions with variable range with the restriction that the shape of the attractive shell is also ellipsoidal (see Fig. 1). The uniform attraction means that the inner hard ellipsoid core is embedded into a square-well shell with $\sigma_{\perp} + \delta\sigma_{\parallel}$ perpendicular and $\sigma_{\parallel}(1 + \delta)$ parallel lengths, where δ denotes the range of the attraction. The corresponding outer aspect ratio and volume to calculate $b_2^O = b(k_o)v_o/v$, are given by $k_o = k \frac{1 + \delta}{1 + k\delta}$ and $v_o = v(1 + k\delta)^2(1 + \delta)$. For the equator attraction case, the ellipsoid core has a surrounding attractive shell with $\sigma_{\perp} + \delta\sigma_{\parallel}$ and σ_{\parallel} ellipsoid lengths. In this case, $k_o = \frac{k}{1 + k\delta}$ is the aspect ratio and $v_o = v(1 + k\delta)^2$ is the volume of the outer shell. Finally, the pole attraction is defined with an enclosing ellipsoid shell with lengths σ_{\perp} and $\sigma_{\parallel}(1 + \delta)$. Therefore the corresponding aspect ratio and volume are given by $k_o = k(1 + \delta)$ and $v_o = v(1 + \delta)$. Note that the uniform attraction has the largest attractive volume from these three cases, implying that its critical temperature must be the highest. To be consistent with previous studies [24, 28], it is worth rewriting Eq. (10) into the following form

$$\frac{1}{T_c^*} = \ln \left\{ 1 - \frac{B_{2,c}^A / B_2^H}{B_2^O / B_2^H - 1} \right\}, \quad (15)$$

where $B_2^O / B_2^H = \frac{b(k_o)v_o}{b(k)v}$ and $B_{2,c}^A / B_2^H$ is given by Eq. (14). Using Eqs. (9), (11), and (14)

we can calculate the critical temperature from Eq. (15) for any ellipsoid shape. We present the shape dependence of the critical temperature in Fig. 3 for some aspect ratios and attractive shells. As expected, the highest critical temperatures belong to the uniform attraction at a given attractive range (δ), while the pole attraction produces the lowest T_c^* . It can also be seen that the shape of the curves changes from concave to convex with increasing δ , which appears clearly in the spherical limit. Surprisingly, the agreement between the theory and simulation is good for all types of attractions. For example, the second virial perturbation theory, which inherits B_2 exactly, is approximate for short-ranged attractions ($0 < \delta < 0.25$) even if B_2 constitutes the basis of the

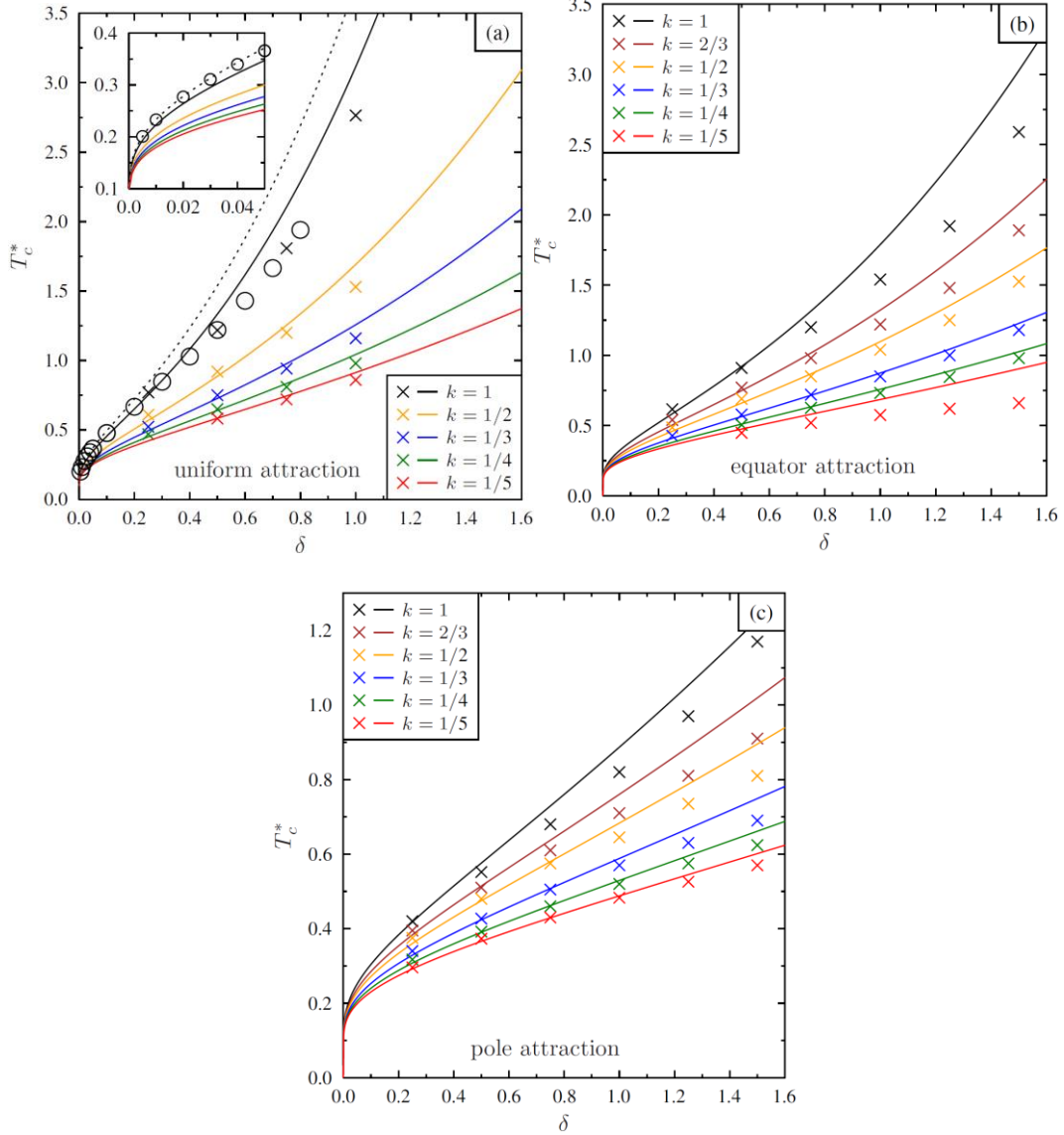


Figure 3. Critical temperature ($T_c^* = k_B T_c / \varepsilon$) of attractive oblate ellipsoids as a function of attractive range (δ). The cross symbols show our REMC simulation results, while the circles are the short-ranged square-well simulation outcomes of [24]. The continuous curves are the results of the second virial perturbation theory (see Eq. (15)). The dashed curve represents Eq. (15) with $B_{2,c}^A / B_2^H = -2.174$ and $k=1$, which was determined with MC simulations for short-ranged square-well interaction [28]. Types of ellipsoid attractions: uniform (a), equatorial (b), and pole (c).

ELCS. Consequently, the theory underestimates T_c^* compared to simulations for spherical particles with short-ranged attraction (see the inset of Fig. 3 (a)). It is worth mentioning that the exact results can be reproduced very accurately by substituting $B_{2,c}^A / B_2^H = -2.174$ into Eq. (15) [28]. As the perturbation theory underestimates the value of $B_{2,c}^A / B_2^H$ for spherical shapes, and

probably for $k \neq 1$, too, the theoretical critical temperature is slightly lower than the simulated one (see Fig. 3 at $\delta=0.25$). At intermediate attraction ranges ($0.25 < \delta < 0.75$), the agreement between theory and simulation is quite good, since the theoretical and simulation critical temperatures cross each other in this range of attraction. It is also not surprising that the theory overestimates the critical temperature in the range of $0.75 < \delta < 1.5$, because this is a common feature of mean-field theories for intermediate attraction ranges. However, the theoretical and simulation critical temperatures get closer to each other with increasing δ , because the theory turns exact in the mean-field limit ($\delta \rightarrow \infty$). So the second virial perturbation theory serves the worst result around $\delta=1.5$ (see Fig. 3). Note that $B_{2,c}^A / B_2^H$ is never constant but proportional to δ even for very short-ranged attractions [28]. Hence, the ELCS is true only on the level of the second virial perturbation theory, where $B_{2,c}^A / B_2^H$ is a constant for all attraction shells.

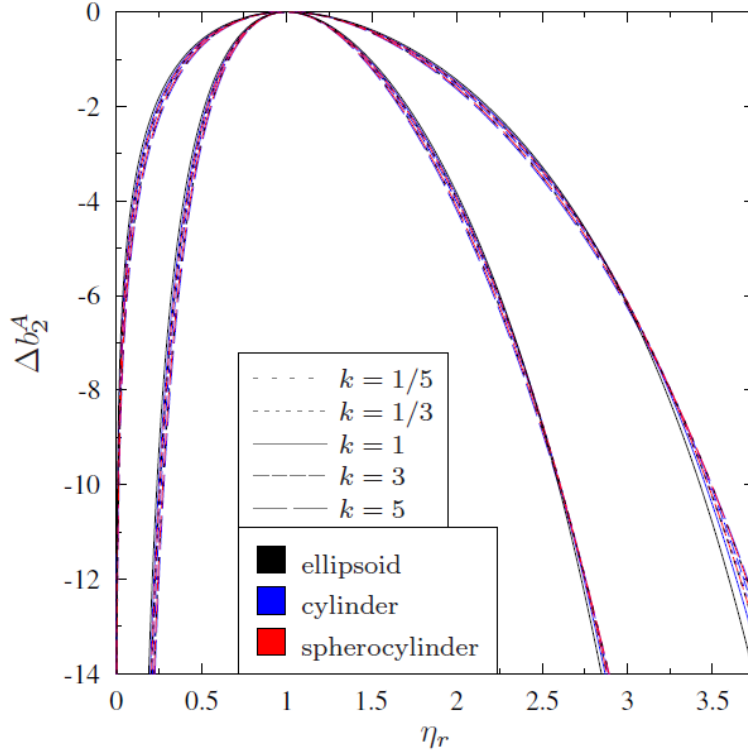


Figure 4. Vapor-liquid spinodal and binodal curves of non-spherical particles in $\Delta b_2^A = b_2^A - b_{2,c}^A$ vs. $\eta_r = \eta / \eta_c$ plane. The outer curves are binodals and the inner ones are spinodals. The examined shapes of the bodies are ellipsoid, cylinder, and spherocylinder. The curves are the results of the second virial perturbation theory using $b_2(k)$ of different shapes.

The spinodal of the VL transition is given by Eq. (6), where only b_2^H carries information about the shape and the aspect ratio of the particle, while the properties of the attraction are built

into b_2^A . Therefore b_2^A vs. η curves form a master curve for a given shape and aspect ratio, where the shape, the thickness, and the depth of the outer attractive shell do not affect the spinodal. As $b_{2,c}^A$ and η_c change with varying shape and k , we shift the position of all critical points into the same one by plotting $\Delta b_2^A := b_2^A - b_{2,c}^A$ as a function of reduced density ($\eta_r = \eta/\eta_c$). With this shift, the location of the critical point is always at $\Delta b_2^A = 0$ and $\eta_r = 1$ for any shape and k . Fig. 4 shows the spinodal and binodal curves together for ellipsoids, cylinders, and spherocylinders. We can see that the curves of ellipsoids are identical for k and $1/k$ pairs due to the oblate-prolate symmetry of b_2^H . In contrast to ellipsoids, the Δb_2^A vs. η_r curves do not coincide for oblate and prolate cylinders because of the lack of $k \leftrightarrow 1/k$ symmetry. In the case of spherocylinders, the results are shown for $k \geq 1$, since they cannot be oblates. We can see that the Δb_2^A vs. η_r curves do not collapse into a single one, i.e. there is no shape and aspect ratio independent master curve. On the vapor side we can observe a definite trend in the binodals (spinodals) as the curves move right with increasing k . Conversely, the liquid binodal (spinodal) curves cross each other, where η_r is between 2.5 and 3.5. Note that the crossing points among the binodals occur still in the liquid phase as the packing fraction of isotropic-nematic and fluid-solid transitions is usually above $3\eta_c$. In addition, it can be seen in Fig. 4 that all binodals stay together more or less up to $\eta \approx 3\eta_c$ for all examined shapes in the range of $1/5 < k < 5$, which suggests that the Δb_2^A vs. η_r curves collapse into a quasi-master curve for non-spherical particles with square-well attraction. In order to see the deviation in the VL binodals more clearly in Fig. 4, we transform our fluids into a reference spherical square-well fluid with a mapping from η_r into a reference reduced packing fraction (η_{rs}). To determine η_{rs} we prescribe a correspondence between non-spherical particles and spheres via $\Delta b_2^A(\eta_r, k) = \Delta b_2^A(\eta_{rs}, k=1)$, which provides η_{rs} as a function of k and η_r . With this mapping, the spinodals and binodals of non-spherical particles become identical with those of spherical particles in the Δb_2^A vs. η_{rs} plane. The benefit of this mapping is that we get the correction $\Delta\eta_r = \eta_{rs} - \eta_r$ as a function of η_r , which is shown in Fig. 5. One can see that corrections to η_r are negative on the vapor side and both negative and positive signs of corrections on the liquid side. Note that there is no need for correction around $\eta_r = 3$, which manifests in a cross point in Fig. 4. More importantly, these corrections are always small for $1/5 < k < 5$, which is good news indeed. Therefore we conclude that the Δb_2^A vs. η_r representation of the VL phase coexistence is a very good way to give rise to the collapse in spinodal and binodal data for different shapes and aspect ratios.

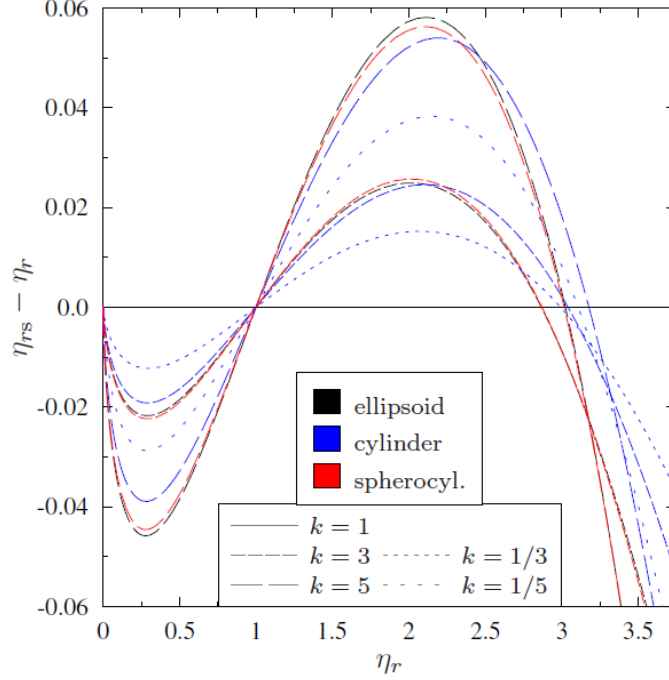


Figure 5. The required shift in the reduced packing fraction of VL binodals of non-spherical particles to collapse with the VL binodal of spherical ones. The curves are presented for ellipsoids, cylinders, and spherocylinders.

In the following, we search for an even better collapse of the binodals by examining the third order virial expansion of the hard body contribution together with the second virial perturbation theory for the attraction. In this approximation the free energy density is given by

$$\frac{\beta F}{N} = \ln \eta - 1 + b_2^H \eta + b_3^H \eta^2 + b_2^A \eta, \quad (16)$$

where b_3^H is the reduced third virial coefficient of the non-spherical hard body. Starting from this equation we get that $\eta_c = 1/\sqrt{6b_3^H}$ and $b_{2,c}^A = -b_2^H - \sqrt{6b_3^H}$. Using these critical quantities, we can prove that the vapor ($\eta_{r,V}$) and liquid ($\eta_{r,L}$) reduced densities of the coexisting phases obey the following two equations

$$\Delta b_2^A \eta_c = \frac{-1 + \eta_{r,V} + \eta_{r,L} - \frac{1}{3}(\eta_{r,V}^2 + \eta_{r,L}\eta_{r,V} + \eta_{r,L}^2)}{\eta_{r,V} + \eta_{r,L}}, \quad (17)$$

$$\Delta b_2^A \eta_c = 1 - \frac{\eta_{r,V} + \eta_{r,L}}{4} - \frac{1}{2} \frac{\ln(\eta_{r,L}/\eta_{r,V})}{\eta_{r,L} - \eta_{r,V}}.$$

We can see from Eq. (17) that $\eta_{r,V}$ and $\eta_{r,L}$ do not depend on the shape and k , because $\Delta b_2^A \eta_c$ is only a function of η_r . Therefore all binodals coincide in the $\Delta b_2^A \eta_c - \eta_r$ plane on the level of this approximation. For the vapor branch, Fig. 6 compares the outcomes of Eq. (16) with those of Eq. (2). We can observe that the binodal coming from Eq. (16) does not collapse with those coming from Eq. (2) for different k values, because the contributions of higher order terms are not negligible even on the vapor side. However, Fig. 6 justifies that the vapor branches of the binodals are almost k independent in the $\Delta b_2^A \eta_c - \eta_r$ plane. Considering the liquid branch, Eq. (17) is not reliable because the density is high. In spite of this, we checked the binodals coming from Eq. (2) in the $\Delta b_2^A \eta_c$ vs. η_r plane. We observed that this representation worsen the collapse of the binodals, since the curves diverge from each other with increasing density, and the crossing points disappear. Additionally, we found that the simulation data of the vapor branch do not exhibit a significant improvement in the collapse using the $\Delta b_2^A \eta_c$ vs. η_r representation. In brief, we cannot justify the findings of Eq. (16) with simulations.

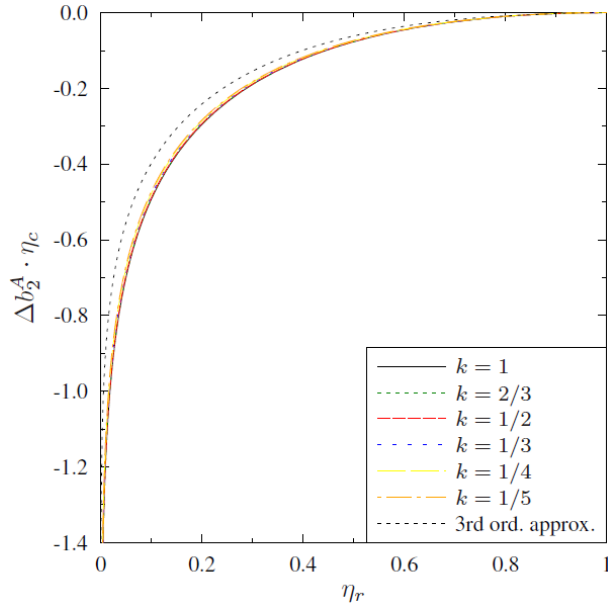


Figure 6. Vapor side of the binodal curve of square-well oblate ellipsoids in the $\Delta b_2^A \eta_c$ vs. $\eta_r = \eta/\eta_c$ plane. The curves are the results of the second virial perturbation theory.

From the above analysis we found that the best collapse of the binodals can be achieved in the Δb_2^A vs. η_r plane. To justify this, we present our REMC simulation data in Fig. 7 for the binodals of oblate ellipsoids in this representation. Several combinations of k and δ values are

considered for pole, equator, and uniform attractions, where $k=1, 2/3, 1/2, 1/3,$ and $1/5,$ and $\delta=0.25, 0.5, 0.75, 1, 1.25,$ and $1.5.$ In summary, we have determined the vapor-liquid binodals of 84 different systems to check the prediction of the perturbation theory for the Δb_2^A vs. η_r curves [59]. For comparison, we have added an inset in Fig. 7, where we have followed the classical $T_r = T/T_c$ vs. η_r representation. We can see in this inset that the collapse of different systems is very poor in the VDW picture, which is in sharp contrast with the representation of the same data in the Δb_2^A vs. η_r plane (see the main panel of Fig. 7). This observation strongly suggests that η_r and Δb_2^A play major roles in the phase behavior of anisotropic particles. For the hypothetical case of $\beta F / N = f(\eta_r, \Delta b_2^A)$ dependence, $\Delta b_2^A = \Delta b_2^A(\eta_r)$ would provide the master curve of all systems, and $z = \beta P / \rho$ would depend on η_r and Δb_2^A , which would constitute a new principle of corresponding states. However, it is not possible to incorporate all microscopic interactions into the second virial coefficient and the reduced density. So the free energy has a complex dependence on the particle parameters, i.e. $\beta F / N = f(\eta, \varepsilon, \delta, k, \dots)$ and $\Delta b_2^A = \Delta b_2^A(\eta_r, \delta, k, \dots)$ cannot collapse perfectly in the Δb_2^A vs. η_r plane.

In the light of good collapse of the VL data in Fig. 7, we decided to construct an approximate master curve with the following formula for both vapour ($0 < \eta_r < 1$) and liquid ($\eta_r > 1$) branches

$$\Delta b_2^A = \begin{cases} (a+b)^{-1} - (a\eta_r^3 + b\eta_r^{1/2})^{-1} & 0 < \eta_r < 1 \\ -c(\eta_r - 1)^7 - d(\eta_r - 1)^2 & 1 < \eta_r \end{cases} . \quad (18)$$

Note that we ensure that both branches yield $\Delta b_2^A = 0$ for $\eta_r=1$. Using the Levenberg-Marquardt method, we first determined not only the values of a, b, c and d , but the exponents, too. We found that the values of the exponents are very close to 3 and 1/2 in the vapour branch and to 7 and 2 in the liquid branch. Therefore we fixed the values of the exponents to the values seen in Eq. (18) and we made a second fit for a, b, c and d . We found the best fit with $a= 6.5754, b= 0.6575, c= 0.3343,$ and $d= 2.8155$ values, which result is shown in Fig. 7. Using Eq. (18) we can determine accurately the VL binodals of arbitrary oblate square-well ellipsoids. For example, knowing the coexistence packing fractions η_V and η_L at a given temperature T^* from a single simulation run, one can get the critical packing fraction by equating the vapor and liquid sides of Eq. (18), i.e.

$$(a+b)^{-1} - (a(\eta_V / \eta_c)^3 + b(\eta_V / \eta_c)^{1/2})^{-1} = -c((\eta_L / \eta_c) - 1)^7 - d(\eta_V / \eta_c - 1)^2 . \quad (19)$$

Using η_V and η_c (or η_L and η_c) we get the value of Δb_2^A at T^* from Eq. (18), which can be used to obtain the value of $b_{2,c}^A$ as $b_{2,c}^A = b_2^A - \Delta b_2^A$, where $b_2^A = (1 - \exp(1/T^*)) (b_2^O - b_2^H)$. Moreover, we can also determine T_c^* from $b_{2,c}^A = (1 - \exp(1/T_c^*)) (b_2^O - b_2^H)$. Finally, we get the binodal in T^* vs. η plane with the help of Eq. (18) using of the values of $b_{2,c}^A$ and η_c .

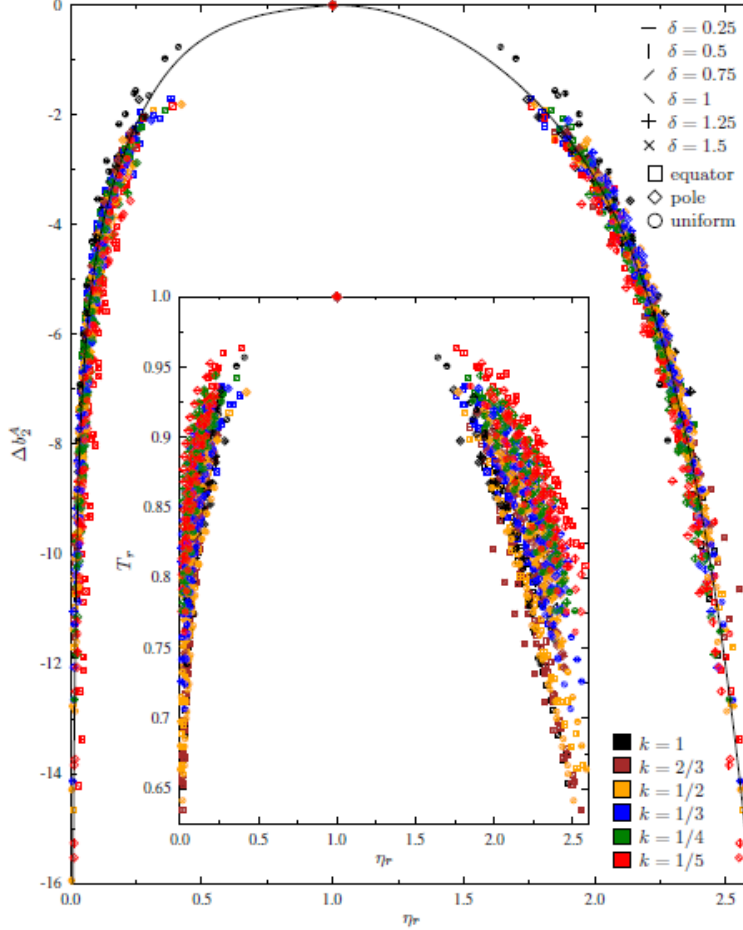


Figure 7. Vapor-liquid binodals of oblate ellipsoids with uniform, equator, and pole square-well attractions in the $\Delta b_2^A = b_2^A - b_{2,c}^A$ vs. $\eta_r = \eta/\eta_c$ plane. The inset shows the usual T_r vs η_r representation of the phase coexistences, where $T_r = T/T_c$. Aspect ratios and attraction ranges are chosen to be in the range of $1/5 < k < 1$ and $0 < \delta < 1.5$. Symbols represent the REMC simulation data, while the continuous curve is the best fit to the data (see Eq. (18)).

Regarding prolate ellipsoids ($k > 1$) and other shapes like the cylinder and spherocylinder, an approximate collapse of the binodals is also expected according to the second virial perturbation theory (see Fig. 4). To check this finding, new simulations should be performed for prolate particles, too. Thus, it remains an open question whether Eq. (18) can be considered as an approximate master curve for non-spherical convex particles of any shape. Moreover, the

validity range of Eq. (18) may exceed $1/5 < k < 1$ but we expect increasing deviations due to the trends observed in Fig 5. We leave these issues for future simulation studies.

VI. Conclusions

The second virial perturbation theory of anisotropic particles suggests that the vapour-liquid binodals of non-spherical particles, which are embedded into attractive wells, can collapse approximately into a master curve in the Δb_2^A vs. η_r plane. This can be true if the main effects of the well-depth, the shape, and the range of attraction are incorporated into the second virial coefficient. We checked this finding by performing a series of simulations for oblate ellipsoids with square-well attractions of variable shape and range. Along this line, we examined three types of enclosing square-well attractions, namely, uniform, equator, and pole attractions, where the shape of the enclosing attraction is always ellipsoidal. Starting from the spherical limit ($k=1$), we scanned the $1/5 < k < 1$ and $0 < \delta < 1.5$ regions. Based on our simulations of 84 different systems, we showed that the best VL data collapse occurs indeed in the Δb_2^A vs. η_r plane in accordance with the theoretical findings. The fitted $\Delta b_2^A = f(\eta_r)$ equation enables us to determine the approximate VL binodal of an oblate ellipsoid system with $1/5 < k < 1$ from a single simulation run, which also provides the coexisting densities at a temperature $T^* < T_c^*$. Therefore our master equation (Eq. (18)) can be used for new simulation studies of oblate particles to get the whole binodal in a very short time. Our perturbation theory says more that the approximate $\Delta b_2^A = f(\eta_r)$ master curve can be used for other convex shapes like cylinders and spherocylinders, where the particles can be both oblate ($k < 1$) and prolate ($k > 1$). This statement is based on the observation that the attractive part of the second virial coefficient, which incorporates the details of the attractive interaction, governs mainly the thermodynamic behaviour of anisotropic fluids for both short and long-ranged attractions. On the one hand, b_2^A includes the contribution of the attraction exactly in the sticky limit of spherical square-well pair potential, i.e. the compressibility factor ($z = \beta P / \rho$) depends on η and b_2^A only [26]. On the other hand, the second virial perturbation theory becomes identical to the exact mean field theory in the long-range attraction limit, where $\delta \rightarrow \infty$ and $\varepsilon \rightarrow 0$ [2]. Even though b_2^A constitutes a bridge between the sticky and the long-range attraction limits, we cannot conclude from this study that the attraction parameters affects exclusively the thermodynamic behavior through b_2^A , because the VL binodals do not collapse in the b_2^A vs. η plane. Thus, the effects of k and δ cannot be incorporated totally into b_2^A , and z is a complicated function of the potential parameters, i.e. $z = z(\eta, b_2^A, k, \delta, \dots)$. This convoluted dependence excludes the possibility of finding a new principle of corresponding states and a master curve in the plane of reduced quantities. Therefore it is not possible to define a reduced density, temperature, and pressure, where different systems obey the same reduced equation of state. Note that even the ELCS does not fulfill the principle as

$z = z(\eta, b_2^A, \delta)$, and the corresponding binodals do not collapse perfectly into a single master curve in the b_2^A - η plane. For example, the critical value of b_2^A has a linear dependence on δ for very short-ranged square-well fluids [28]. The case of non-spherical particles is more complicated in this regard as both the shape and the aspect ratio of hard-cores and the attractive shells affect the critical behavior of anisotropic fluids. At this point, it is worth noticing that both v and B_2^H are equally good to make B_2^A dimensionless for spherical particles as $B_2^H = 4v$. This is simply not true for non-spherical particles, because B_2^H is not proportional to v anymore implying that the master curve with B_2^A / B_2^H differs from that of $b_2^A = B_2^A / v$. We found that b_2^A provides a much better collapse of the binodals than B_2^A / B_2^H in agreement with our perturbation theory. Note that the second virial perturbation theory satisfies exactly the ELCS for a given aspect ratio, where the reduced quantities are η and b_2^A .

The ELCS is generalized for patchy particles, where the attraction is strongly directional dependent [34]. It was observed in the system of patchy hard spheres that the critical value of B_2^A / B_2^{HS} has a very strong dependence on the number of patches (M). It was found for very short-ranged patches that $B_{2,c}^A / B_2^{HS} = -27.71$ for $M=3$, and $B_{2,c}^A / B_2^{HS} = -4.03$ for $M=5$. With increasing M , we get closer to the sticky hard sphere limit, where the system loses its directional character. Thus, $B_{2,c}^A / B_2^{HS}$ increases and converges to $B_{2,c}^A / B_2^{HS} = -2.174$ with increasing M . In our study the particle's aspect ratio (k) makes both the repulsive and attractive interactions directional. One may naively expect that k plays a similar role to M . We observed that η_c goes to zero in the $k \rightarrow \infty$ or $k \rightarrow 0$ limits, where $B_{2,c}^A / B_2^H = -1$ (see Eq. (14)). Consequently, the effect of k is very different from M as $B_{2,c}^A / B_2^H$ increases from -2.65 to -1 with increasing the shape anisotropy. From these results, we can see that the critical behavior of patchy non-spherical particles differs substantially from that of the square-well ellipsoids.

Based on the previous paragraphs, we can conclude that our study has predictive power for the VL phase coexistence of nonspherical convex particles embedded into a square-well attraction. In addition, it is worth mentioning that the ELCS is also fulfilled for spherical and soft potentials [60, 61], i.e. it is likely that the law could also be applied for nonspherical and soft pair potentials such as the Kihara [62] and the Gay-Berne [63], where the VL binodals would also depend on the shape anisotropy. Finally, it would also be interesting to examine the validity of the principle of corresponding states in two dimensions like the system of hard ellipses embedded into square-well shells [64].

Acknowledgments

The authors thank financial support of CONACyT project A1-S-9197. VS and GP acknowledge the National Research, Development, and Innovation Office-K 137720 for financial support.

References

- [1] J. A. Barker and D. Henderson, *Rev. Mod. Phys.* 48, 587 (1976).
- [2] J. P. Hansen and I. R. McDonald, *Theory of Simple Liquids*, 3rd ed. (Academic, London, 2006).
- [3] J. A. Barker and D. Henderson, *J. Chem. Phys.* 47, 2856 (1967).
- [4] J. A. Barker and D. Henderson, *J. Chem. Phys.* 47, 4714 (1967).
- [5] I Szalai and J Liszi, *Berichte der Bunsengesellschaft für physikalische Chemie* 97, 1054 (1993).
- [6] A. Gil-Villegas, F. del Rio and A. L. Benavides, *Fluid Phase Equilibria*, 119, 97 (1996).
- [7] A. Gil-Villegas, A. Galindo, P. J. Whitehead, S. J. Mills, G. Jackson, and A. N. Burgess, *J. Chem. Phys.* 106, 4168 (1997).
- [8] S. Varga, D. Boda, D. Henderson, and S. Sokolowski, *J. Colloid and Interface Science* 227, 223 (2000).
- [9] M. Lozada-Cassou, R. Saavedra-Barrera, and D. Henderson, *J. Chem. Phys.* 77, 5150 (1982).
- [10] M. Lozada-Cassou and D. Henderson, *J. Phys. Chem.* 87, 2821 (1983).
- [11] E. Gonzales-Tovar, M. Lozada-Cassou, and D. Henderson, *J. Chem. Phys.* 83, 361 (1985).
- [12] M. Lozada-Cassou and D. Henderson, *Chem. Phys. Lett.* 127, 392 (1986).
- [13] D. Henderson and M. Lozada-Cassou, *J. Colloid and Interface Science* 114, 180 (1986).
- [14] D. Henderson, *Fundamentals of Inhomogeneous Fluids* 1st Edition, CRC Press (1992).
- [15] D. Henderson, S. Sokolowski, and Darsh Wasan, *J. Stat. Phys.* 89, 233 (1997).
- [16] A. Trokhymchuk, I. Nezbeda, J. Jirsák and D. Henderson, *J. Chem. Phys.* 123, 024501 (2005).
- [17] A. Huerta, D. Henderson and A. Trokhymchuk, *Phys. Rev. E* 74, 061106 (2006).
- [18] D. Henderson, *Mol. Phys.* 30, 971 (1975).
- [19] T. Boublík, *Mol. Phys.* 109, 1575 (2011).
- [20] D. Henderson and P. J. Leonard, *Proceeding of the National Academy of Sciences*, 68, 632 (1971).
- [21] E. A. Guggenheim, *J. Chem. Phys.* 13, 253 (1945).
- [22] K. E. Pitzer, *J. Chem. Phys.* 7, 583 (1939).
- [23] G. A. Vliegenthart and H. N. W. Lekkerkerker, *J. Chem. Phys.* 112 5364 (2000).
- [24] M. G. Noro and D. Frenkel, *J. Chem. Phys.* 113, 2941 (2000).

- [25] R. J. Baxter, *J. Chem. Phys.* 49 2770 (1968).
- [26] M. A. Miller and D. Frenkel, *J. Chem. Phys.* 121, 535 (2004).
- [27] D. Gazzillo, *J. Chem. Phys.* 134, 124504 (2011).
- [28] J. Largo, M. A. Miller and F. Sciortino, *J. Chem. Phys.* 128, 134513 (2008).
- [29] A. Malijevský, S. B. Yuste and A. Santos, *J. Chem. Phys.* 125, 074507 (2006).
- [30] P. Orea, C. Tapia-Medina, D. Pini, and A. Reiner, *J. Chem. Phys.* 132, 114108 (2010).
- [31] N. E. Valadez-Pérez, A. L. Benavides, E. Schöll-Paschinger and R. Castañeda-Priego, *J. Chem. Phys.* 137, 084905 (2012).
- [32] E. Schöll-Paschinger, N. E. Valadez-Pérez, A. L. Benavides and R. Castañeda-Priego, *J. Chem. Phys.* 139, 184902 (2013).
- [33] F. Platten, N. E. Valadez-Pérez, R. Castañeda-Priego, and S. U. Egelhaaf, *J. Chem. Phys.* 142, 174905 (2015).
- [34] G. Foffi and F. Sciortino, *J. Phys. Chem. B* 111 9702 (2007).
- [35] G. Foffi, C. D. Michele, F. Sciortino, and P. Tartaglia, *Phys. Rev. Lett.* 94, 078301 (2005).
- [36] N. E. Valadez-Pérez, Y. Liu and R. Castañeda-Priego, *Phys. Rev. Lett.* 120, 248004 (2018).
- [37] G. Foffi and F. Sciortino, *Phys. Rev. E* 74, 050401 (2006).
- [38] P. Orea, S. Varga, and G. Odriozola, *Chem. Phys. Lett.*, 631, 26 (2015).
- [39] M. Gómez de Santiago, P. Gurin, S. Varga, and G. Odriozola, *J. Phys.: Condens. Matter* 34, 104002 (2022).
- [40] W. R. Smith, D. Henderson, and R. D. Murphy, *J. Chem. Phys.* 61, 2911 (1974).
- [41] A. L. Benavides, F. Del Rio, *Mol. Phys.* 68, 983 (1989).
- [42] P. Orea, Y. Duda, V. C. Weiss, W. Schröer and J. Alejandre, *J. Chem. Phys.* 120, 11754 (2004).
- [43] B. P. Patel, H. Docherty, S. Varga, A. Galindo and G. C. Maitland, *Mol. Phys.* 103, 129 (2005).
- [44] D. L. Pagan and J. D. Gunton, *J. Chem. Phys.* 122, 184515 (2005).
- [45] R. López-Rendón, Y. Reyes, and P. Orea, *J. Chem. Phys.* 125, 084508 (2006).
- [46] R Espíndola-Heredía, F del Río, and A Malijevsky, *J. Chem. Phys.* 130, 024509 (2009).
- [47] J. D. Parsons, *Phys. Rev. A* 19, 1225 (1979).

- [48] S. D. Lee, *J. Chem. Phys.* 87, 4972 (1987).
- [49] B. Tjipto-Margo and G. T. A. Evans, *Mol. Phys.* 74, 85 (1991); A. Samborski and G. T. Evans, *Mol. Phys.* 80 1257 (1993).
- [50] S. Varga, I. Szalai, J. Liszi, and G. Jackson, *J. Chem. Phys.* 116, 9107 (2002).
- [51] G. S. Singh and B. Kumar, *J. Chem. Phys.* 105, 2429 (1996).
- [52] L. Onsager, *Ann. N.Y. Acad. Sci.* 51, 627 (1949).
- [53] E. Herold, R. Hellmann, and J. Wagner, *J. Chem. Phys.* 147, 204102 (2017).
- [54] A. P. Lyubartsev, A. A. Martsinovski, S. V. Shevkunov, and P. N. Vorontsov-Velyaminov, *J. Chem. Phys.* 96, 1776 (1992).
- [55] E. Marinari and G. Parisi, *Europhys. Lett.* 19, 451 (1992).
- [56] K. Hukushima and K. Nemoto, *J. Phys. Soc. Japan* 65, 1604 (1996).
- [57] G. A. Chapela, G. Saville, S. M. Thompson and J. S. Rowlinson, *J. Chem. Soc. Faraday Trans. II* 73, 1133 (1977).
- [58] A. Donev, S. Torquato and F. H. Stillinger, *J. Comput. Phys.* 202, 737 (2005).
- [59] The vapour-liquid binodal data of REMC simulations are collected together in the supplementary material.
- [60] P. Orea, A. Romero-Martínez, E. Basurto, C. A. Vargas, G. Odriozola, *J. Chem. Phys.* 143, 024504 (2015).
- [61] J. L. Salazar and Y. Reyes, *J. Mol. Liq.*, 294, 111606 (2019).
- [62] T. Kihara, *J. Phys. Soc. Jpn.* 6, 289 (1951).
- [63] J. G. Gay and B. J. Berne, *J. Chem. Phys.* 74, 3316 (1981).
- [64] R. Melnyk, Y. Kalyuzhnyi, G. Kahl, and A. Baumketner, *J. Chem. Phys.* 156, 034102 (2022).